International Journal of Disaster Risk Reduction 42 (2020) 101352

Contents lists available at ScienceDirect

International Journal of Disaster Risk Reduction

journal homepage: http://www.elsevier.com/locate/ijdrr

Numerical analysis of tsunami-triggered oil spill fires from petrochemical industrial complexes in Osaka Bay, Japan, for thermal radiation hazard assessment

Tomoaki Nishino [a,*], Youhei Takagi [b]

[a] Disaster Prevention Research Institute, Kyoto University, Gokasho, Uji, Kyoto 611-0011, Japan
[b] Yokohama National University, Tokiwadai 79-5, Hodogaya-ku, Yokohama 240-8501, Japan

ARTICLE INFO

Keywords:
Fire following tsunami
Oil spill
Natech
Hazard map
Tsunami vertical evacuation
Nankai trough subduction zone

ABSTRACT

This study assesses thermal radiation hazards from tsunami-triggered oil spill fires from petrochemical industrial complexes in Japan, and demonstrates that the assessment provides useful results for understanding how large an area will be exposed to high thermal radiation, and which tsunami vertical evacuation buildings will be in danger from the fires. A tsunami-triggered oil spill fire spread model was applied for the Port of Osaka, which has approximately 360 ha of petrochemical industrial complexes. A tsunami following a hypothetical magnitude 8.6 earthquake along the Nankai Trough subduction zone was considered. Oil spills caused by the tsunami and fire spread over oil were numerically simulated for several scenarios by varying the initial ignition location and time. Hazard maps representing the spatial distribution of maximum radiant heat flux from the fires were created. The calculations showed that one tsunami vertical evacuation building was exposed to a radiant heat flux of 40 kW/m^2 or more in the worst-case scenario. Therefore, this building is likely to be ignited by the fires, and it is recommended that this building be used as little as possible for tsunami vertical evacuation. In addition, ten tsunami vertical evacuation buildings, which are not likely to be ignited, would, in several scenarios, be exposed to a radiant heat flux that exceeds the minimum heat flux that causes human skin burns. Therefore, when rooftops of these buildings are used for refuge areas, measures for shielding these areas from thermal radiation need to be implemented, such as mounting parapet walls on rooftops.

1. Introduction

The Tohoku earthquake had a moment magnitude of 9.0 and occurred off the coast of Japan in 2011. This earthquake has generated new challenges for preparedness against fires following tsunami in Japan, where fires following earthquakes have been of major concern. The massive tsunami following the earthquake struck wide areas of Tohoku and Kanto, and caused 124 fires in tsunami inundation areas [1]. The fires were incomparably larger in number than the tsunami-triggered fires in past earthquakes in Japan, such as the 1964 Niigata earthquake and the 1993 Hokkaido earthquake. Hazardous flammable materials released by the tsunami were presumed to be major contributing factors to the occurrence of fires in tsunami inundation areas [2]. In particular, as much as 7530 kL of marine diesel oil was spilled from storage tanks in Kesennuma City, Miyagi Prefecture, by the tsunami, which had a height of up to 6 m off the coast of the city, and inundated an area of approximately 18 km^2. Subsequently, the oil spill triggered large-scale fires that spread over Kesennuma Bay as shown in Fig. 1, and the fires affected some of the tsunami vertical evacuation buildings in the city [3,28]. According to previous fire experiments, burning wooden debris is presumed to ignite the oil floating on the sea by acting as a candle wick [4]. Because a megathrust earthquake similar to the Tohoku earthquake is expected to occur along the Nankai Trough subduction zone off the coast of Japan at some point in the future [30], there are concerns that a massive tsunami will trigger large-scale oil spill fires in coastal cities that have petrochemical industrial complexes. Since the 2003 Tokachi-oki earthquake, it has been recommended that oil storage tanks in Japan should reduce the amount of products in storage in order to prevent oil spill due to liquid sloshing caused by long-period ground motions [27]. However, sufficient preparedness against tsunami-triggered oil spill fires has not been achieved because of the lack of hazard assessment. In particular, tsunami vertical evacuation

* Corresponding author.
E-mail address: nishino.tomoaki.3c@kyoto-u.ac.jp (T. Nishino).

https://doi.org/10.1016/j.ijdrr.2019.101352
Received 10 June 2019; Received in revised form 1 October 2019; Accepted 1 October 2019
Available online 8 October 2019

Fig. 1. Tsunami-triggered oil spill fires that spread over Kesennuma Bay, Miyagi Prefecture, Japan, after the 2011 Tohoku earthquake: the photograph was taken by Ryosuke Onodera from the rooftop of a tsunami vertical evacuation building.

buildings, which are known to be effective risk reduction options for coastal communities without accessible high ground [5,6], have been designated in great numbers without consideration of fires following tsunami since the Tohoku earthquake. Some tsunami vertical evacuation buildings are likely to be affected by fires in the vicinity of petrochemical industrial complexes.

Assessing thermal radiation hazards from tsunami-triggered oil spill fires is expected to be useful for gaining an understanding of how large an area will be exposed to high thermal radiation and which tsunami vertical evacuation buildings will be in danger from fires. Because natural hazard triggered technological (Natech) disasters have been of major concern [7,8], several researchers have analyzed hazardous material releases triggered by tsunamis. Cruz et al. [9] analyzed the potential consequences of tsunami scenarios and their impact on an oil refinery using numerical simulation of tsunami propagation and inundation. Krausmann and Cruz [10] analyzed the impact of the tsunami following the 2011 Tohoku earthquake on chemical industries by collecting accident information from open sources and conducting interview surveys. Kyaw et al. [11] numerically simulated the spread of oil from industrial parks at Osaka Bay, Japan, caused by a tsunami following an earthquake in the Nankai Trough subduction zone. However, few studies have analyzed subsequent fires and thermal radiation hazards. Therefore, Nishino and Imazu [3] have developed a model for numerically simulating oil spills caused by tsunamis and fire spread over oil (hereinafter called the "tsunami-triggered oil spill fire spread model"), and simulated the fires that spread over Kensennuma Bay after the Tohoku earthquake to validate the model. Because the burning behavior of fires spreading over tsunami-driven oil was physically modeled, this model appeared to be applicable to the assessment of thermal radiation hazards from tsunami-triggered oil spill fires.

The present study assesses thermal radiation hazards from tsunami-triggered oil spill fires from petrochemical industrial complexes in Japan in order to investigate how large an area will be exposed to high thermal radiation and to identify which tsunami vertical evacuation buildings will be in danger from the fires. The tsunami-triggered oil spill fire spread model was applied to the Port of Osaka, which is one of the major international trading ports in Japan and has approximately 360 ha of petrochemical industrial complexes. A tsunami following a hypothetical magnitude 8.6 earthquake along the Nankai Trough subduction zone was considered. Oil spills caused by the tsunami and fire spread over oil were numerically simulated for several scenarios by varying the initial ignition location and time. Hazard maps that represent the spatial distribution of maximum radiant heat flux from the fires were created.

2. Study area

Fig. 2 shows the location of the study area and the tsunami source model used in this study. The Port of Osaka is located in the northern area of Osaka Bay, Japan, and is approximately 200 km from the Nankai Trough, which lies in a subduction zone between the Eurasian and Philippine Sea plates off the coast of Japan, and has a length of approximately 700 km. The petrochemical industrial complexes, which have a total of 237 oil storage tanks, are distributed along the coast close to the urban areas of Osaka, which is the second largest city in Japan. A number of buildings are designated as tsunami vertical evacuation buildings by the local government of Osaka City. They were essentially constructed after 1982 from reinforced concrete or steel reinforced concrete, and are three stories or more high. The Central Disaster Management Council [12,13], under the auspices of the Cabinet Office of the Japanese Government, has developed several tsunami source models for megathrust earthquakes along the Nankai Trough subduction zone. Therefore, one tsunami source model for a hypothetical magnitude 8.6 earthquake [29], called the Tonankai-Nankai earthquake, was selected for simulating tsunami propagation and inundation in this study. In the tsunami source model, a fault plane is divided into small dislocations, and the slip on each dislocation is given so that the model simulates estimated tsunami heights for the past earthquakes.

Oil storage tank behavior under tsunami inundation can be roughly classified into six possible types as shown in Fig. 3 [32]; floating, sliding, tumbling, side-buckling by internal pressure rise, bottom-plate separation by inclining, and side-buckling by inclining. The Osaka Prefecture [14] has estimated the amount of oil spilled from the oil storage tanks in the petrochemical industrial complexes by floating and sliding caused by a tsunami. Floating and sliding are particularly important oil spill mechanisms because of the tsunami wave force and buoyancy. The estimated amount of oil spilled was up to 27,227 kL of petroleum products, such as gasoline, kerosene, fuel oil, and lubricating oil. This is because few measures have been implemented to protect oil storage tanks from tsunami inundation, although measures have been applied to protect oil storage tanks from seismic ground motion.

3. Methodology

Thermal radiation hazards from tsunami-triggered oil spill fires were assessed by sequentially conducting three kinds of numerical simulations for (1) tsunami propagation and inundation, (2) oil spills caused by tsunami and fire spread over oil, and (3) thermal radiation from fires.

3.1. Tsunami propagation and inundation

A tsunami simulator based on computational fluid dynamics (STOC-ML), which has been developed by Tomita et al. [15], was used for numerically simulating the tsunami propagation and inundation. STOC-ML is a quasi-three-dimensional model based on hydrostatic approximations, in which the fluid body can be divided into multiple layers in the depth direction, and has been validated by comparing the calculated results with the tsunami waveforms recorded at tide stations in the 2011 Tohoku earthquake. Initial water surface elevation caused by the deformation of the sea bottom, which is needed for simulating the tsunami propagation and inundation, was calculated from the tsunami source model parameters using the method of Mansinha and Smylie [19]. Four nested domains, with grid sizes of 1350 m, 450 m, 150 m, and 50 m, respectively, were applied to the computational domains from the fault to land as shown in Fig. 4. Although a grid size of 10 m is usually used for simulating tsunami inundation in urban areas, a grid size of 50 m seemed to be adequate for the simulation in this study because most of the spilled oil was expected to be carried into the bay by the tsunami and contribute to fires there. Free transmission and zero

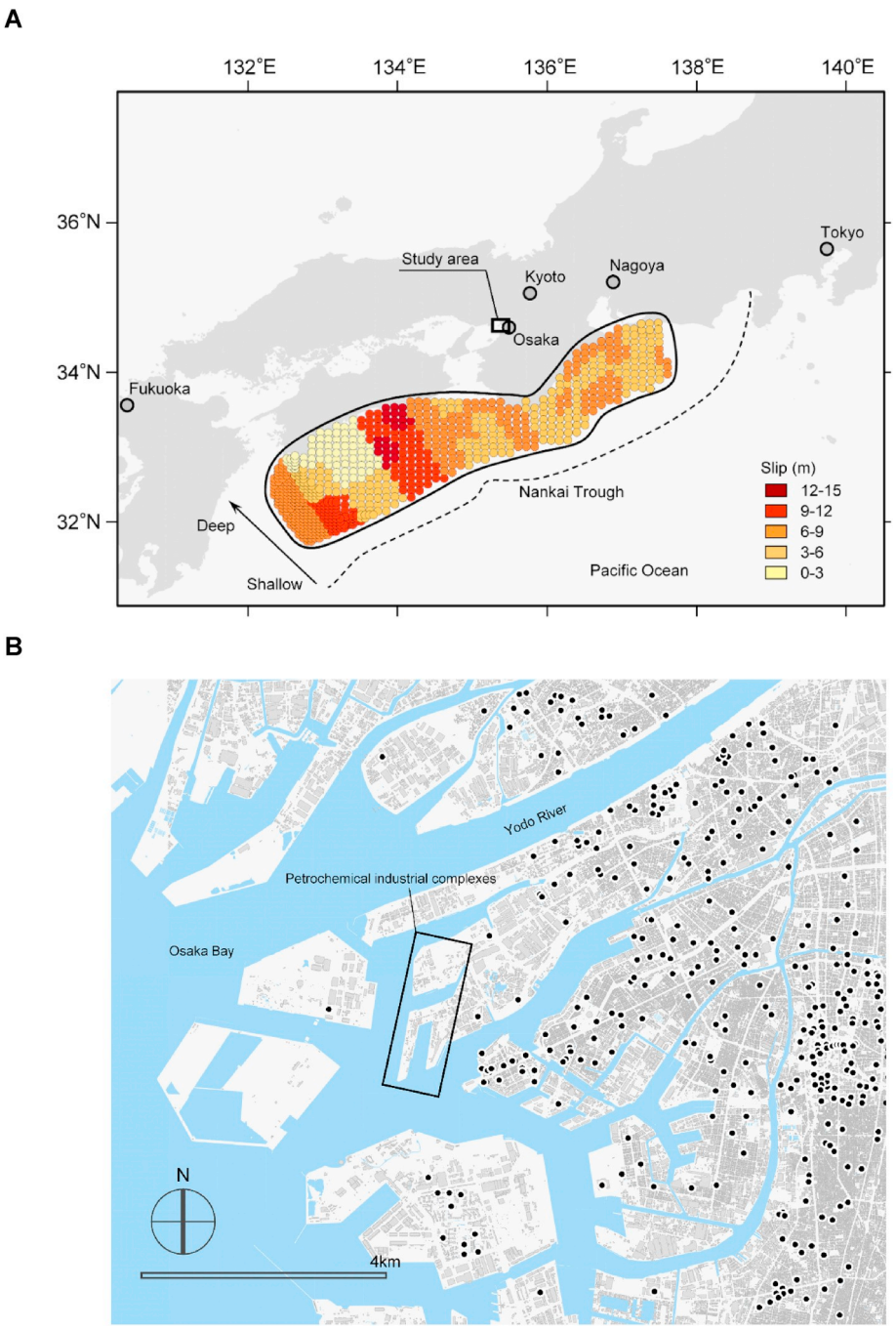

Fig. 2. Overview of the study area: (A) the location of the Port of Osaka and the tsunami source model for a hypothetical magnitude 8.6 earthquake along the Nankai Trough subduction zone [29], (B) the location of petrochemical industrial complexes in the Port of Osaka and tsunami vertical evacuation buildings (plotted in black) designated by the local government of Osaka City. The arrow shown in (A) represents the depth direction along the subduction zone.

gradient boundary conditions were applied at the outer edge of computational domains for water surface elevation and water velocity, respectively. Topography (ground elevation) and bathymetry data published by the Cabinet Office of the Japanese Government were used. Bottom friction at the sea floor was considered using Manning's formula and its coefficient of roughness. Resistance of structures on land was also considered using Manning's formula, and the coefficient of roughness was selected according to the type of the land use. The effects of seawalls were neglected because it was assumed that seawalls would be destroyed by seismic ground motion before the tsunami hits, that is, the analysis is based on a worst-case scenario. If the seawalls remain standing and are not overtopped by the tsunami, the oil spill fires will be smaller than those indicated by the results of this study. The effects of gates were also neglected in the worst-case scenario. The time increment was set to 0.6 s by considering the Courant-Friedrichs-Lewy condition.

The governing equations used in STOC-ML [15] consist of a continuity equation that describes the conservation of mass, and Navier–-Stokes equations that describe the conservation of momentum:

$$\frac{\partial}{\partial x}(\gamma_x u)+\frac{\partial}{\partial y}(\gamma_y v)+\frac{\partial}{\partial z}(\gamma_z w)=0 \quad (1)$$

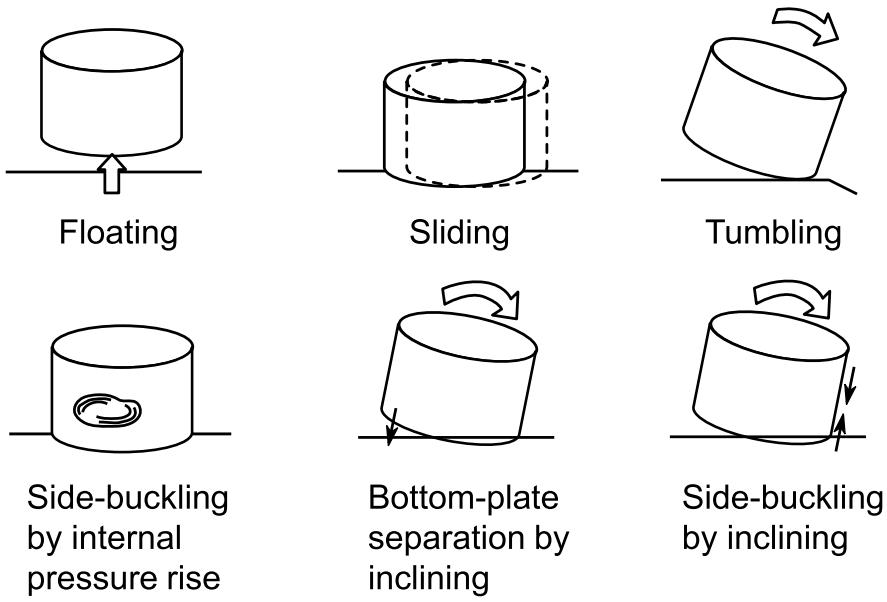

Fig. 3. Classification of oil storage tank behavior under tsunami inundation [32].

$$\gamma_v\frac{\partial u}{\partial t}+\frac{\partial}{\partial x}(\gamma_x uu)+\frac{\partial}{\partial y}(\gamma_y vu)+\frac{\partial}{\partial z}(\gamma_z wu)-f_0 v$$
$$=-\gamma_v\frac{1}{\rho}\frac{\partial p}{\partial x}+\frac{\partial}{\partial x}\left(\gamma_x\nu_e 2\frac{\partial u}{\partial x}\right)+\frac{\partial}{\partial y}\left\{\gamma_y\nu_e\left(\frac{\partial u}{\partial y}+\frac{\partial v}{\partial x}\right)\right\}+\frac{\partial}{\partial z}\left\{\gamma_z\nu_e\left(\frac{\partial u}{\partial z}+\frac{\partial w}{\partial x}\right)\right\} \quad (2)$$

$$\gamma_v\frac{\partial v}{\partial t}+\frac{\partial}{\partial x}(\gamma_x uv)+\frac{\partial}{\partial y}(\gamma_y vv)+\frac{\partial}{\partial z}(\gamma_z wv)+f_0 u$$
$$=-\gamma_v\frac{1}{\rho}\frac{\partial p}{\partial y}+\frac{\partial}{\partial x}\left\{\gamma_x\nu_e\left(\frac{\partial v}{\partial x}+\frac{\partial u}{\partial y}\right)\right\}+\frac{\partial}{\partial y}\left(\gamma_y\nu_e 2\frac{\partial v}{\partial y}\right)+\frac{\partial}{\partial z}\left\{\gamma_z\nu_e\left(\frac{\partial v}{\partial z}+\frac{\partial w}{\partial y}\right)\right\} \quad (3)$$

$$\gamma_v\frac{\partial w}{\partial t}+\frac{\partial}{\partial x}(\gamma_x uw)+\frac{\partial}{\partial y}(\gamma_y vw)+\frac{\partial}{\partial z}(\gamma_z ww)$$
$$=-\gamma_v g-\gamma_v\frac{1}{\rho}\frac{\partial p}{\partial z}+\frac{\partial}{\partial x}\left\{\gamma_x\nu_e\left(\frac{\partial w}{\partial x}+\frac{\partial u}{\partial z}\right)\right\}+\frac{\partial}{\partial y}\left\{\gamma_y\nu_e\left(\frac{\partial w}{\partial y}+\frac{\partial v}{\partial z}\right)\right\}+\frac{\partial}{\partial z}\left(\gamma_z\nu_e 2\frac{\partial w}{\partial z}\right) \quad (4)$$

where x and y are the rectangular coordinates in horizontal two dimensions, z is the vertical coordinate, u, v, and w are the fluid velocities of water in the $x-$, $y-$, and $z-$ directions, respectively, t is the time, ρ is the water density, p is the pressure, g is the gravity acceleration, f_0 is the Coriolis coefficient, γ_v is the volume fraction of water in each computational cell, γ_x, γ_y, and γ_z are the area fractions of water in surfaces of each computational cell, and ν_e is the effective kinematic viscosity coefficient. In these equations, the volume fraction of water and the area fractions of water are introduced to improve the prediction accuracy for computational cells located in the vicinity of sea bottoms and structures [17]. The effective kinematic viscosity coefficient ν_e is given by the eddy viscosity coefficient in the Smagorinsky turbulence model [25].

The water surface elevation η is calculated by the following equation, which is obtained by integrating the continuity equation from the bottom to the surface:

$$\gamma_v\frac{\partial \eta}{\partial t}+\frac{\partial}{\partial x}\int_{-h}^{\eta}\gamma_x u dz+\frac{\partial}{\partial y}\int_{-h}^{\eta}\gamma_y v dz=0 \quad (5)$$

where h is the still water depth.

The pressure p is given by the following hydrostatic equation:

$$p=\rho g(\eta-z) \quad (6)$$

3.2. Oil spills caused by tsunami and fire spread over oil

The tsunami-triggered oil spill fire spread model (Fig. 5), which has been developed by Nishino and Imazu [3], was used for numerically simulating oil spills caused by tsunami and fire spread over oil. In this model, tsunami-triggered oil spill fires are regarded as an assemblage of disc-shaped burning oil particles floating on water; temporal locations were calculated in a horizontal two-dimensional coordinate system on the basis of tsunami flow velocities by considering oil spills from multiple locations. The burning zone, which was determined for each burning oil particle, was assumed to have expanded uniformly, regardless of the direction from the center of each burning oil particle, at a rate depending on the thickness. Fire spread from a burning oil particle to an unburned oil particle was assumed to occur when the burning zone was in contact with the unburned oil particle. The rate of heat release by combustion was calculated for each burning oil particle to predict the radiant heat flux from the fires, and the rate of volume loss by combustion was also calculated. The fire was assumed to be extinguished when the oil particle thickness became smaller than 1 mm. The initial ignition, which is unpredictable, was assumed to occur in a single location in the same manner as the past tsunami-triggered oil spill fires in Japan. For example, in the 1964 Niigata earthquake, the fire started in a single location from suspected heat release in a chemical reaction between metal and seawater, and spread over oil spilled in the tsunami inundation area [31]; in the 2011 Tohoku earthquake, the fire also started in a single location from suspected burning floating debris, and spread over oil floating on the bay [28]. However, there is a possibility

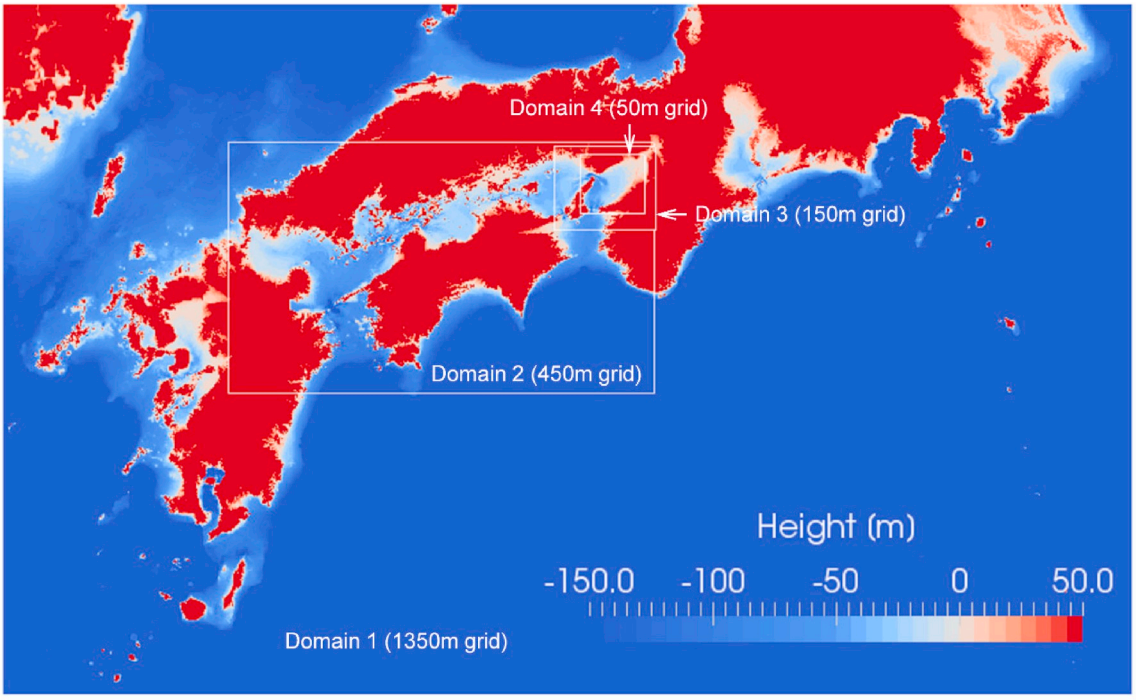

Fig. 4. Four nested domains used for the tsunami propagation and inundation simulation.

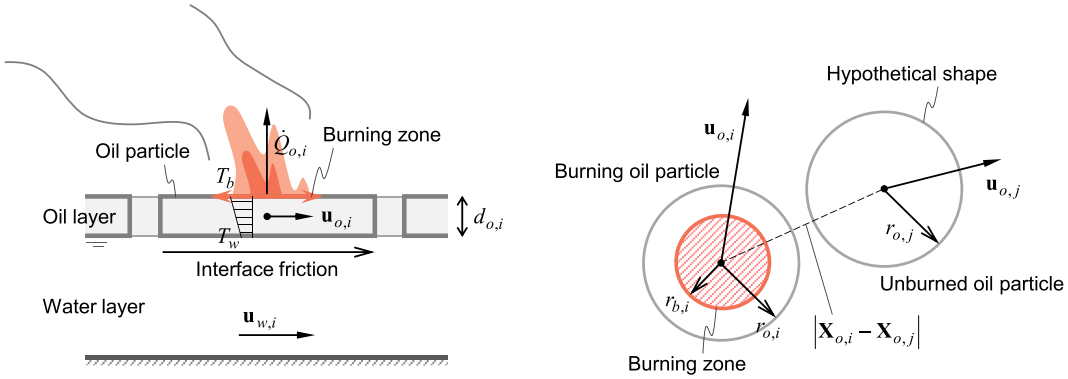

Fig. 5. Schematic of a tsunami-triggered oil spill fire spread model [3].

that multiple initial ignitions occur at various locations. In the present study, the initial ignition was provided by the initial burning of an oil particle by randomly selecting an oil particle and specifying the ignition time.

The amount of oil spilled was based on the results estimated by the Osaka Prefecture [14]. However, gasoline is expected to vaporize immediately after being spilled, and a total of 22,404 kL of petroleum products excluding gasoline, such as kerosene, fuel oil, and lubricating oil, were considered as the oil spilled. The initial oil particle volume was set to 0.05 m^3, and consequently, a total of 448,080 oil particles were considered. For simplicity, the properties of oil particles, which are expected to be mixtures of different petroleum products, were approximated by the properties of fuel oil that is expected to be spilled the most. The oil spill locations were set to 197 points to correspond with oil storage tank locations in Osaka. However, these number and locations are slightly different from the number and locations reported by the Osaka Prefecture because the present study determined the locations of oil storage tanks by scanning aerial photographs. The amount of oil spilled was assumed to be equally distributed among the oil storage tanks as the contents of the tanks. The oil spill was assumed to start at 126 min after the earthquake regardless of location, when the water surface elevation was predicted to reach the maximum height around the petrochemical industrial complexes. The rate of oil spill was set to 0.2 m^3/s regardless of location by assuming that there was a small crack on the surface of each oil storage tank.

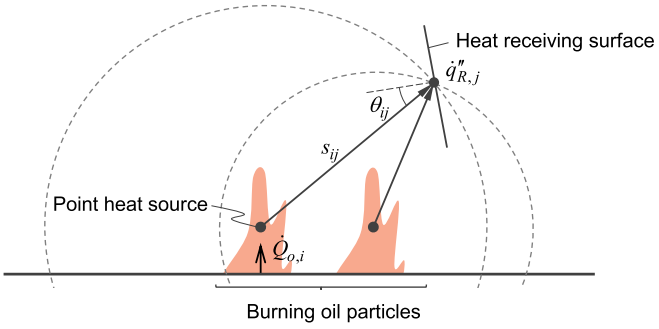

Fig. 6. Schematic of a simple calculation method for radiant heat flux from fires by isotropic radiation approximation.

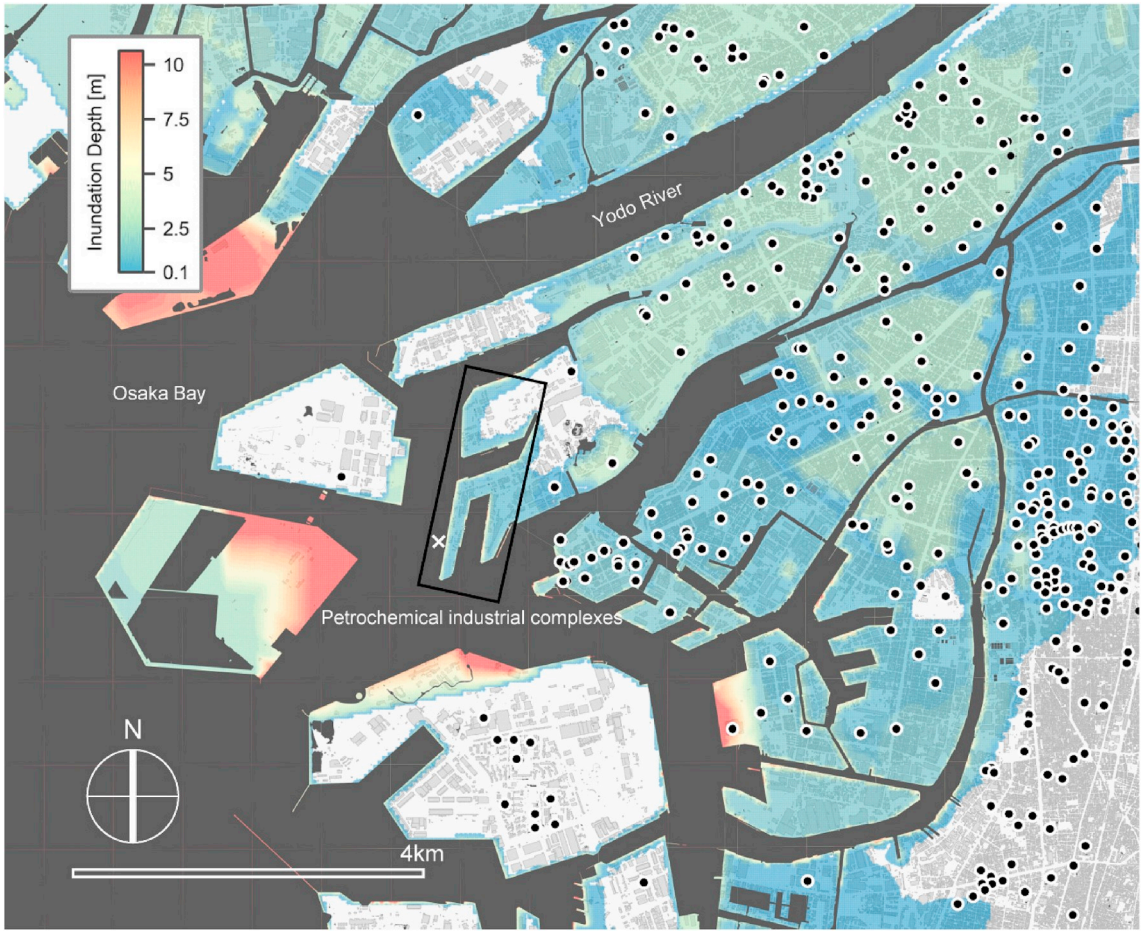

Fig. 7. Inundation depth calculated by a tsunami simulator (STOC-ML). Tsunami vertical evacuation buildings designated by the local government of Osaka City are plotted in black.

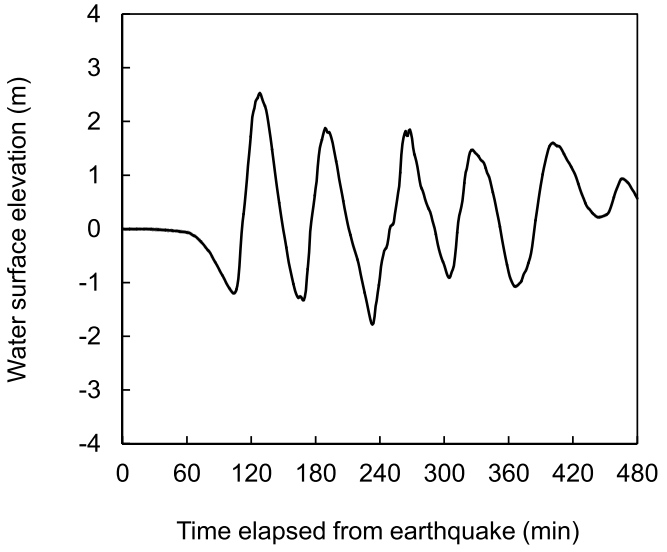

Fig. 8. Tsunami waveform calculated at a specific location near the petrochemical industrial complexes by the tsunami simulator (STOC-ML). The location of the calculated tsunami waveform is shown with a cross in Fig. 7.

3.2.1. Oil particle location and shape

The oil particle location $\mathbf{X}_{o,i}$ is given by the following equations, in which the displacement is assumed to be the sum of (1) the deterministic displacement resulting from the interface friction between oil and water and (2) the probabilistic displacements that describe the effect of the turbulence in water and the effect of the oil spreading caused by gravity and viscous force:

$$\mathbf{X}_{o,i} = \mathbf{X}^{I}_{o,i} + \int_{t_{s,i}}^{t} \mathbf{u}_{o,i} dt + \Delta\mathbf{X}_{w,i} + \Delta\mathbf{X}_{s,i} \tag{7}$$

$$\frac{\partial \mathbf{u}_{o,i}}{\partial t} = C_f \frac{1}{d_{o,i}} (\mathbf{u}_{w,i} - \mathbf{u}_{o,i}) \left| \mathbf{u}_{w,i} - \mathbf{u}_{o,i} \right| \tag{8}$$

$$\Delta\mathbf{X}_{w,i} = \sum_{k=m_{s,i}}^{m} \left(\begin{bmatrix} \sqrt{24\kappa_{x,i}\Delta t} & 0 \\ 0 & \sqrt{24\kappa_{y,i}\Delta t} \end{bmatrix} \begin{bmatrix} \xi_{1,i} - \frac{1}{2} \\ \xi_{2,i} - \frac{1}{2} \end{bmatrix} \right) \tag{9}$$

$$\Delta\mathbf{X}_{s,i} = C_p (t - t_{s,i})^{1/4} \sqrt{\Delta t} \begin{bmatrix} \cos(2\pi\xi_{3,i}) \\ \sin(2\pi\xi_{4,i}) \end{bmatrix} \tag{10}$$

where i is the identification mark for each oil particle, $\mathbf{u}_{o,i}$ is the oil particle velocity resulting from the interface friction between oil and water, $\mathbf{u}_{w,i}$ is the water velocity, $\mathbf{X}^{I}_{o,i}$ is the initial oil particle location, $\Delta\mathbf{X}_{w,i}$ is the probabilistic displacement that describes the effect of the turbulence in water, $\Delta\mathbf{X}_{s,i}$ is the probabilistic displacement that describes the effect of the oil spreading caused by gravity and viscous

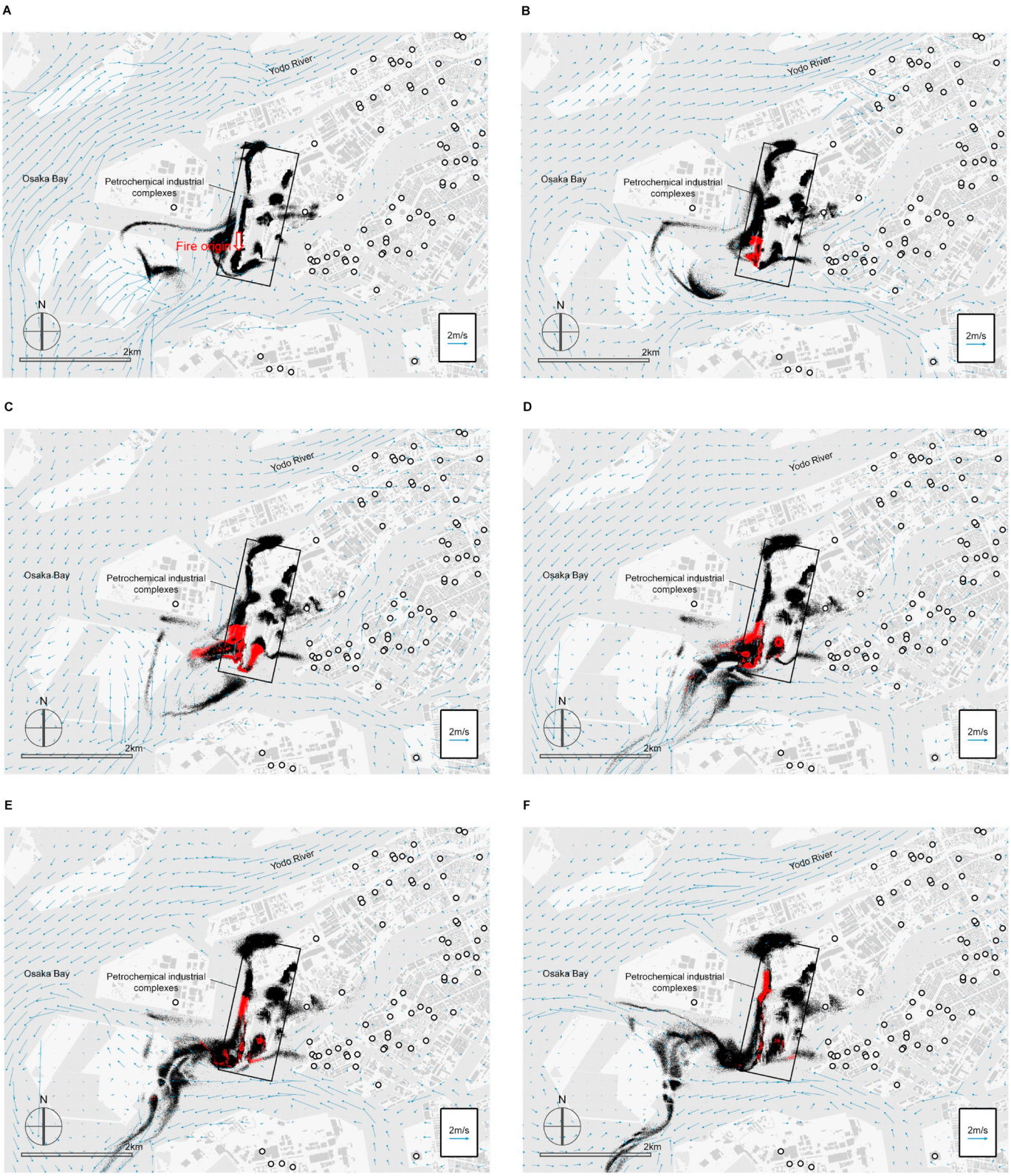

Fig. 9. Calculation example of the dynamic state of tsunami-triggered oil spill fires: (A) 180 min, (B) 190 min, (C) 200 min, (D) 210 min, (E) 220 min, (F) 230 min, (G) 240 min, (H) 250 min, and (I) 260 min after the earthquake. The fire was assumed to break out at 180 min after the earthquake. Arrows represent water velocity vectors calculated by STOC-ML. Black particles and red particles represent unburned oil particles and burning oil particles, respectively. Black circles on white represent tsunami vertical evacuation buildings designated by the local government of Osaka City. (For interpretation of the references to colour in this figure legend, the reader is referred to the Web version of this article.)

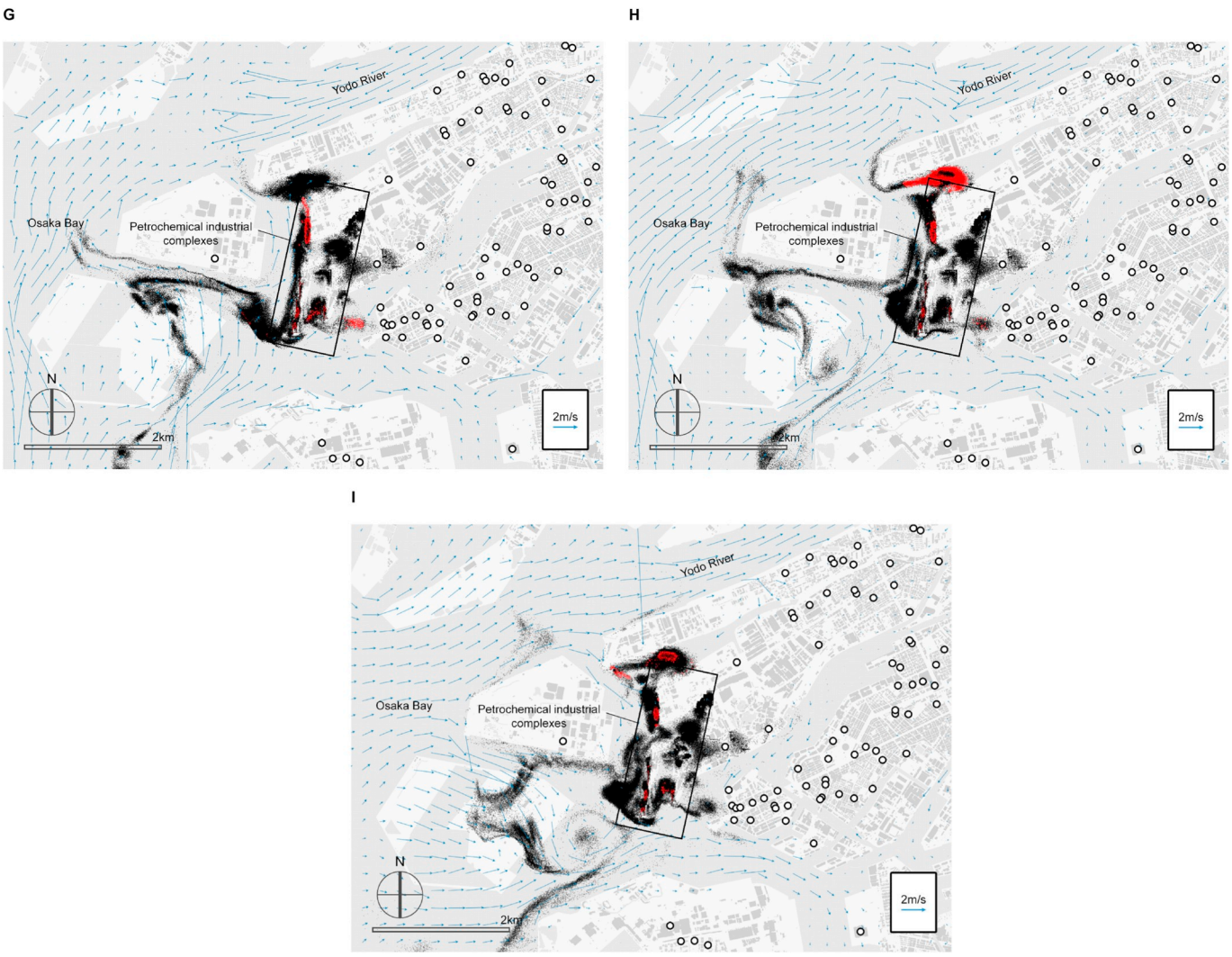

Fig. 9. (*continued*).

force, $d_{o,i}$ is the oil particle thickness, C_f is the friction coefficient (0.006 was used, based on the hydraulic experiments conducted by Lau and Moir [20]), C_p is the spreading coefficient (0.115 was used, based on the hydraulic experiments conducted by Matsuzaki and Fujita [21]), $\kappa_{x,i}$ and $\kappa_{y,i}$ are the diffusion coefficients calculated based on the hydraulic experiments conducted by Elder [22], $t_{s,i}$ is the start time of the spill, Δt is the time increment, m is the number of steps, $m_{s,i}$ is the number of steps corresponding to the start time of the spill, and $\xi_{1,i}$, $\xi_{2,i}$, $\xi_{3,i}$ and $\xi_{4,i}$ are uniform random numbers between 0 and 1 and were calculated using a multiplicative linear congruential generator [26].

The oil particle thickness $d_{o,i}$ is given by the following equation, which calculates the average thickness for each cell in mesh $\overline{d_k}$:

$$d_{o,i} \equiv \overline{d_k}, \quad \overline{d_k} = \sum_{i=1}^{n_o} \delta_{ik} V_{o,i} \Big/ b^2 \tag{11}$$

where n_o is the number of oil particles, k is the identification mark for each cell, $V_{o,i}$ is the oil particle volume, δ_{ik} is a dummy variable that is 1 if an oil particle i exists in the cell k and 0 if it does not, and b is the cell width.

The oil particle radius $r_{o,i}$ is given by the following equation:

$$r_{o,i} = \sqrt{\frac{A_{o,i}}{\pi}} = \sqrt{\frac{V_{o,i}/d_{o,i}}{\pi}} \tag{12}$$

3.2.2. Oil particle fire behavior

The heat release rate by combustion $\dot{Q}_{o,i}$ is given by the following equation for each burning oil particle by assuming that the burning zone on each oil particle expands uniformly, regardless of direction from the center, at a rate depending on the thickness, and by assuming that the fire is extinguished when the oil particle thickness becomes smaller than 1 mm:

$$\dot{Q}_{o,i} = \Delta H_o \left[\dot{m}''_{b,pool} - \frac{1}{L_v} \left\{ \frac{k_o (T_b - T_w)}{d_{o,i}} \right\} \right] \left(\pi r_{b,i}^2 \right) \tag{13}$$

$$\frac{\partial r_{b,i}}{\partial t} = \begin{cases} 1.2 d_{o,i} + 0.0016 & (0.001 \le d_{o,i} < 0.007) \\ 0.01 & (0.007 \le d_{o,i}) \end{cases} \tag{14}$$

where $r_{b,i}$ is the burning zone radius, ΔH_o is the heat of combustion (42,000 kJ/kg was used), $\dot{m}''_{b,pool}$ is the mass loss rate per unit area obtained from pool fire experiments with a sufficiently large diameter (0.045 kg/s/m^2 was used based on the results of combustion experiments conducted by Blinov and Khudyakov [23]), T_b is the boiling point of oil (603 K was used), T_w is the water temperature (283 K was used), k_o is the effective heat transfer coefficient (3.5×10^{-5} kW/m/K was used [3]), and L_v is the heat of vaporization (250 kJ/kg was used).

The rate of volume loss by combustion is given as follows:

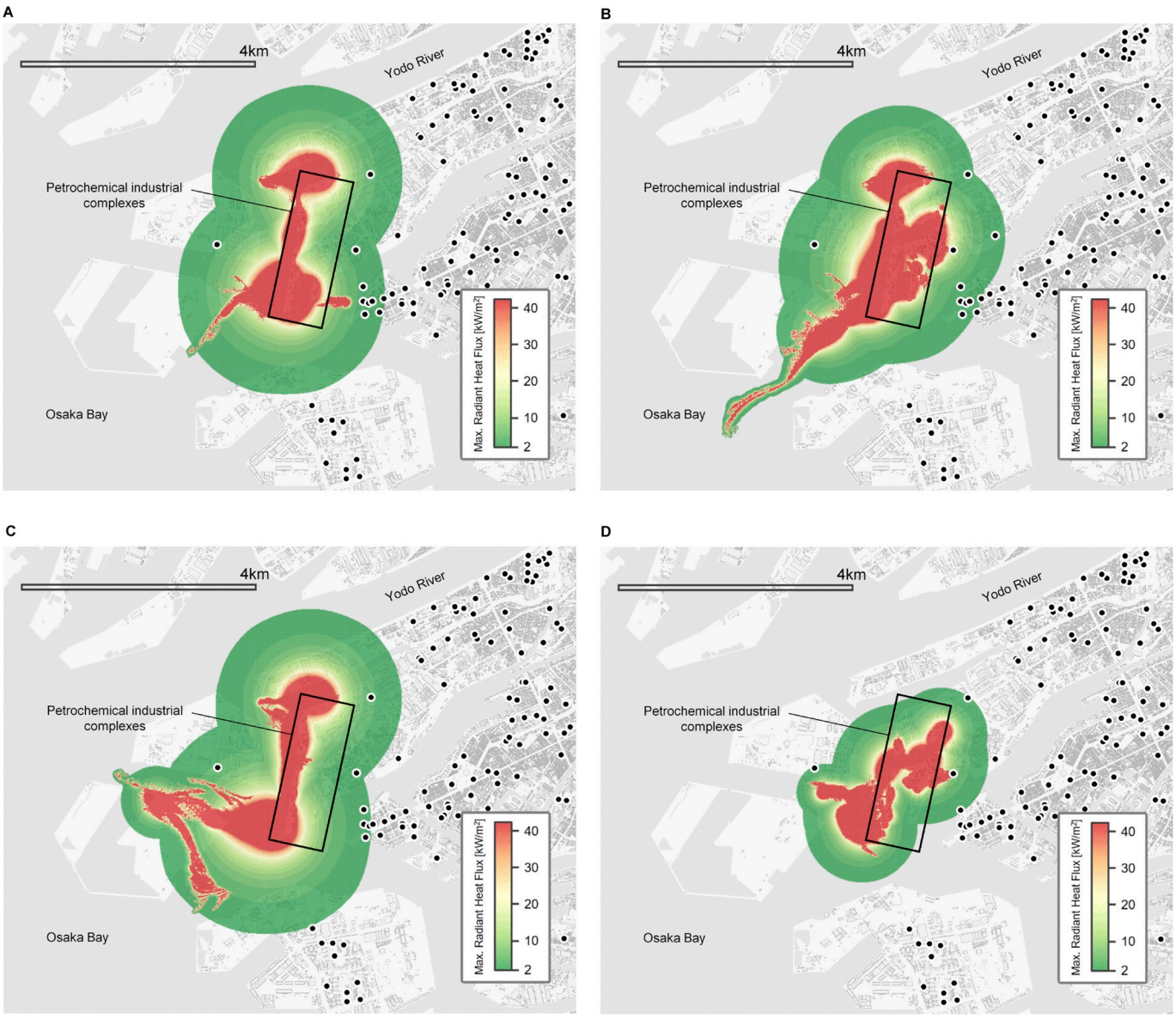

Fig. 10. Hazard maps representing the maximum radiant heat flux at any point in time for each scenario considered. Eight scenarios were considered by varying the initial ignition condition: the initial ignition time was assigned four different values (180 min, 210min, 240 min, and 270 min after the earthquake), and the initial ignition location was varied in two ways for each initial ignition time considered. (A) 180 min-1, (B) 180 min-2, (C) 210 min-1, (D) 210 min-2, (E) 240 min-1, (F) 240 min-2, (G) 270 min-1, and (H) 270 min-2. Tsunami vertical evacuation buildings designated by the local government of Osaka City are plotted in black.

$$\frac{\partial V_{o,i}}{\partial t} = -\left(\frac{\dot{Q}_{o,i}}{\Delta H_o \rho_{o,i}}\right) \tag{15}$$

where $\rho_{o,i}$ is the oil particle density (820 kg/m^3 was used).

Fire spread from a burning oil particle to an unburned oil particle was assumed to occur when the burning zone contacts the unburned oil particle. Letting the burning oil particle and the unburned oil particle be i and j, respectively, the condition for fire spread occurring between oil particles is given by the following equation that considers the positional relationship between two circles:

$$\left|\mathbf{X}_{o,i} - \mathbf{X}_{o,j}\right| \leq r_{b,i} + r_{o,j} \quad \text{and} \quad d_{o,j} \geq 0.001 \tag{16}$$

3.3. Thermal radiation from fires

A simple calculation method, which was developed by Modak [16], was used for predicting the radiant heat flux from the fires (Fig. 6). The radiant heat flux from a flame, which is approximated by a point heat source, was calculated by assuming that the point heat source radiates uniformly in all directions, and the radiant energy passing through a surface at an equal distance from the point heat source is equal to that released from the flame per unit time. This method better predicts the radiant heat flux as the distance from the center of the flame increases or the flame becomes optically thinner. Letting a point heat source and a heat receiving surface with unit area be i and j, respectively, the radiant heat flux from a flame to the heat receiving surface $\dot{q}''_{ij}$ is given by the following equation for each burning oil particle:

$$\dot{q}''_{ij} = \frac{\dot{Q}_{R,i}}{4\pi s_{ij}^2}\cos\theta_{ij} \tag{17}$$

where $\dot{Q}_{R,i}$ is the radiant energy released from a flame per unit time, s_{ij} is the distance between the point heat source and the heat receiving surface, and θ_{ij} is the angle between the outward vector normal to the heat

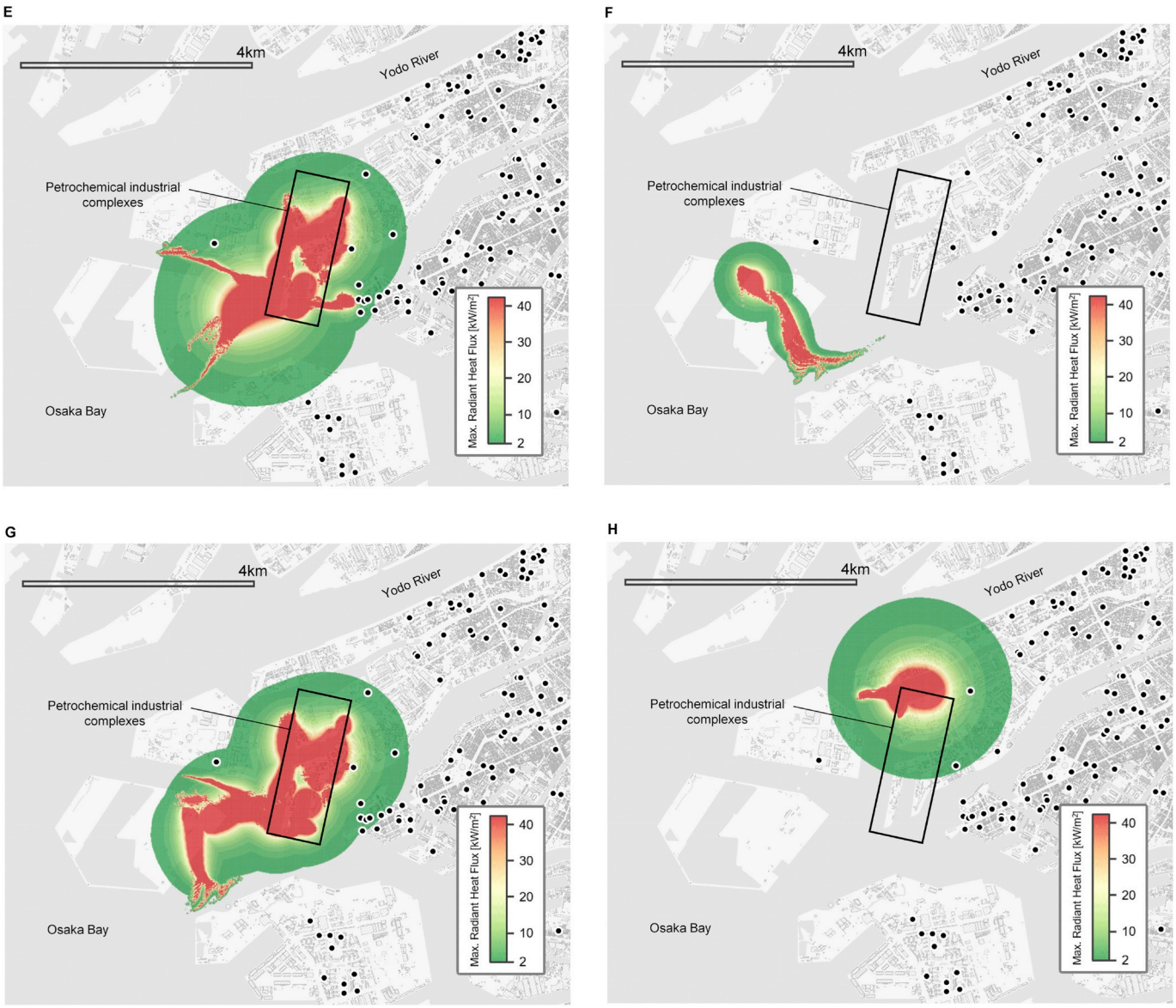

Fig. 10. (*continued*).

receiving surface and the heat ray of radiation.

According to fire experiments by McCaffrey [18], the radiant energy of diffusion flames is approximately 20%–40% of the heat release rate. Thus, the radiant energy released from a flame per unit time $\dot{Q}_{R,i}$ is given as follows:

$$\dot{Q}_{R,i} = \chi_R \dot{Q}_{o,i} \tag{18}$$

where χ_R is the percentage of energy consumed by thermal radiation in the heat release rate (0.3 was used).

The total radiant heat flux from all flames formed above burning oil particles to the heat receiving surface $\dot{q}''_{R,j}$ was calculated using the following equation:

$$\dot{q}''_{R,j} = \sum_{i=1}^{n_b} \left(\frac{\chi_R \dot{Q}_{o,i}}{4\pi s_{ij}^2} \cos\theta_{ij} \right) \tag{19}$$

where n_b is the number of burning oil particles.

To conservatively assess the radiant heat flux from the fires, the radiation shielding by structures was neglected. Moreover, the horizontal distance was substituted into the distance between the point heat source and the heat receiving surface s_{ij}, and the heat receiving surface with unit area was assumed to be a sphere, that is, $\cos\theta_{ij}$ was set to 1.

4. Results and discussion

Fig. 7 shows the inundation depth calculated by the tsunami simulator (STOC-ML). The tsunami rushed to urban areas located several kilometers from the coast; and consequently, a broad area in the vicinity of the Port of Osaka was inundated. The inundation depth within the petrochemical industrial complexes was calculated to be approximately 1 m. Fig. 8 shows the tsunami waveform calculated at a specific location near the petrochemical industrial complexes. The location of the calculated tsunami waveform is shown with a cross in Fig. 7. The water surface elevation reached its maximum height (2.2 m) 126 min after the earthquake. Repeated backwash and anaseism occurred over a period of approximately 60 min.

Fig. 9 shows a calculation example of the dynamic state of tsunami-triggered oil spill fires. In this simulation, the fire was assumed to break out 180 min after the earthquake. At the time of the outbreak of fire, the oil particles were already spilled in the bay from oil storage tanks. However, the oil particles were concentrated near the petrochemical

industrial complexes at this time. After the outbreak, the fire spread to surrounding oil particles one after another and immediately developed into large-scale fires on the bay near the south area of the petrochemical industrial complexes. The average fire spread rate until 200 min after the earthquake (until 20 min after the initial ignition), when the burning area reached its peak, was calculated to be approximately 150 m^2/s. After that, some of the burning oil particles were carried in a northerly direction by the tsunami, and transformed the bay near the northern area of petrochemical industrial complexes into a sea of flames. The tsunami velocity field, which complexly changed over time throughout the fires, greatly affected the dynamic states of the fires.

Fig. 10 shows hazard maps that represent the maximum radiant heat flux at any point in time for each scenario considered. Eight scenarios were considered by varying the initial ignition condition; the initial ignition time was assigned four different values (180 min, 210 min, 240 min, and 270 min after the earthquake), and the initial ignition location was varied in two ways for each initial ignition time considered. The zone exposed to high thermal radiation was calculated to usually occur in and around the petrochemical industrial complexes, although there was great variability in spatial distribution of maximum radiant heat flux. The total area of the high thermal radiation exposure zone was calculated to be up to approximately 16 km^2. However, the zone shows a tendency to be localized when compared with the tsunami inundation zone. As shown in figures B, D, E, and G, one tsunami vertical evacuation building, the nearest evacuation building to the petrochemical industrial complexes, was calculated to be exposed to a radiant heat flux of 20 kW/m^2 or more in several scenarios, and 40 kW/m^2 or more in the worst-case scenario. Therefore, this building is likely to be ignited by the fires, and it is recommended that this building be used as little as possible for tsunami vertical evacuation. In addition, ten tsunami vertical evacuation buildings that are not likely to be ignited by the fires were calculated to be exposed to a radiant heat flux of over 2 kW/m^2 in several scenarios. A radiant heat flux of 2 kW/m^2 is known to be the minimum radiant heat flux that causes human skin burns [24], and has been recommended as the criterion for the planning of urban refuge areas to protect against conflagrations in Japan. Therefore, when rooftops of these buildings are used for refuge areas, measures for shielding these areas from thermal radiation need to be implemented, such as mounting parapet walls on rooftops.

5. Conclusions

A tsunami-triggered oil spill fire spread model was applied to petrochemical industrial complexes in the Port of Osaka, Japan, to assess thermal radiation hazards from the fires. A tsunami following a hypothetical magnitude 8.6 earthquake along the Nankai Trough subduction zone was considered. Oil spills caused by the tsunami and fire spread over oil were numerically simulated for several scenarios by varying the initial ignition location and time. Hazard maps representing the spatial distribution of maximum radiant heat flux from the fires were created. The calculations showed that one tsunami vertical evacuation building was exposed to a radiant heat flux of 40 kW/m^2 or more in the worst-case scenario. Therefore, this building is likely to be ignited by the fires, and it is recommended that this building be used as little as possible for tsunami vertical evacuation. In addition, ten tsunami vertical evacuation buildings that are not likely to be ignited by the fires were calculated to be exposed, in several scenarios, to a radiant heat flux above the minimum heat flux that causes human skin burns. Therefore, when rooftops of these buildings are used for refuge areas, measures for shielding these areas from thermal radiation need to be implemented, such as mounting parapet walls on rooftops.

In contrast to usual cases where only direct impacts of tsunamis on assets are considered, this study investigated secondary impacts of tsunamis due to cascade effects that has not been sufficiently considered. Under the present circumstances where the tsunami-triggered fire risk of tsunami vertical evacuation buildings is neglected in disaster preparedness, this study clarified which the buildings in the Port of Osaka will be in danger from oil spill fires following a possible tsunami and presented recommendations for protecting people from the fires. However, the results are limited because hazard maps were determined for only one possible tsunami scenario. The variability of tsunamis was not discussed in this paper. Other tsunami scenarios will result in different spatial patterns for the hazards. To more comprehensively assess thermal radiation hazards from the fires, a probabilistic hazard assessment methodology needs to be developed that considers the uncertainty of tsunamis as well as the uncertainty of ignitions. Furthermore, the hazard assessment methodology is expected to be useful for assessing additional property damage to the built environment by fires beyond those caused directly by the tsunami. Further research needs to be conducted to analyze impacts of tsunami on properties, including secondary impacts caused by cascade effects.

Acknowledgment

This work was supported by Japan Society for the Promotion of Science Grant-in-Aid for Scientific Research (B) Grant Number 18H01678. We thank Paul Seward, PhD, from Edanz Group (www.edanzediting.com/ac) for editing a draft of this manuscript.

References

[1] A. Sekizawa, K. Sasaki, Study on fires following the 2011 Great East-Japan earthquake based on the questionnaire survey to fire departments in affected areas, Fire Saf. Sci. 11 (2014) 691–703.
[2] A. Hokugo, T. Nishino, T. Inada, Tsunami fires after the great East Japan earthquake, J. Disaster Res. 8 (2013) 584–593.
[3] T. Nishino, Y. Imazu, A computational model for large-scale oil spill fires on water in tsunamis: simulation of oil spill fires at Kesennuma Bay in the 2011 Great East Japan earthquake and tsunami, J. Loss Prev. Process. Ind. 54 (2018) 37–48.
[4] T. Nishino, H. Suzuki, T. Tsuchihashi, Basic experiment on the heat release property of a tsunami fire fueled by debris and fuel oil spilled on the sea surface following tsunami, Fire Saf. Sci. 11 (2014) 758–768.
[5] N. Wood, J. Jones, J. Schelling, M. Schmidtlein, Tsunami vertical-evacuation planning in the U.S. Pacific Northwest as a geospatial, multi-criteria decision problem, Int. J. Disaster Risk Reduct. 9 (2014) 68–83.
[6] J.W. McCaughey, I. Mundir, P. Daly, S. Mahdi, A. Patt, Trust and distrust of tsunami vertical evacuation buildings: extending protection motivation theory to examine choices under social influence, Int. J. Disaster Risk Reduct. 24 (2017) 462–473.
[7] A.M. Cruz, M.C. Suarez-Paba, Advances in Natech research: an overview, Prog. Disaster Sci. 1 (2019), https://doi.org/10.1016/j.pdisas.2019.100013.
[8] S. Girgin, A. Necci, E. Krausmann, Dealing with cascading multi-hazard risks in national risk assessment: the case of Natech accidents, Int. J. Disaster Risk Reduct. 35 (2019) 101072, https://doi.org/10.1016/j.ijdrr.2019.101072.
[9] A.M. Cruz, E. Krausmann, G. Franchello, Analysis of tsunami impact scenarios at an oil refinery, Nat. Hazards 58 (2011) 141–162.
[10] E. Krausmann, A.M. Cruz, Impact of the 11 March 2011, Great East Japan earthquake and tsunami on the chemical industry, Nat. Hazards 67 (2013) 811–828.
[11] W.P. Kyaw, M. Sugiyama, Y. Takagi, H. Suzuki, N. Kato, Numerical analysis of tsunami-triggered oil spill from industrial parks in Osaka Bay, J. Loss Prev. Process. Ind. 50 (2017) 325–336.
[12] Central Disaster Management Council, Report on the Tonankai-Nankai Earthquake, 2003. http://www.bousai.go.jp/kaigirep/chuobou/9/pdf/haifu_2-2.pdf. (Accessed 22 May 2019).
[13] Cabinet Office, Government of Japan, Models for Mega Earthquakes along the Nankai Trough: Tsunami Fault Models, 2012. http://www.bousai.go.jp/jishin/nankai/taisaku/pdf/20120829_2nd_report01.pdf. (Accessed 22 May 2019).
[14] Osaka Prefecture, Disaster Prevention Plan for Petrochemical Industrial Complexes in Osaka, 2017. http://www.pref.osaka.lg.jp/hoantaisaku/bousaikeikaku/bousaikeikakuh2904.html. (Accessed 22 May 2019).
[15] T. Tomita, K. Honda, T. Kakinuma, Application of three-dimensional tsunami simulator to estimation of tsunami behavior around structures, in: Proceedings of 30th International Conference on Coastal Engineering, American Society of Civil Engineers, 2007, pp. 1677–1688.
[16] A.T. Modak, Thermal radiation from pool fires, Combust. Flame 29 (1977) 177–192.
[17] P.L.-F. Liu, P. Lin, K.-A. Chang, T. Sakakiyama, Numerical modeling of wave interaction with porous structures, J. Waterw. Port, Coast. Ocean Eng. 125 (1999) 322–330.
[18] B.J. McCaffrey, Some measurements of the radiative power output of diffusion flames, in: Combustion Institute, Western States Section Meeting, Paper No. WSS/CI 81-15, Pullman, 1981.

[19] L. Mansinha, D.E. Smylie, The displacement fields of inclined faults, Bull. Seismol. Soc. Am. 61 (1971) 1433–1440.
[20] Y.L. Lau, J.R. Moir, Booms used for oil slick control, J. Environ. Eng. Div. - ASCE 105 (1979) 369–382.
[21] Y. Matsuzaki, I. Fujita, Experimental study on mechanical spreading of oil on the water surface and application of numerical simulation, J. Jpn. Soc. Civ. Eng. Series B2 Coast. Eng. 70 (2014) 471–475 (in Japanese).
[22] J.W. Elder, The dispersion of marked fluid in turbulent shear flow, J. Fluid Mech. 5 (1959) 544–560.
[23] V.I. Blinov, G.N. Khudyakov, Diffusion Burning of Liquids, Izdatel'stvo Akademii Nauk SSSR, Moscow. English Translation, U.S. Army Engineering Research and Development Laboratories, Information Resources Branch, Translation Analysis Section, Fort Belvoir, VI, No. T-1490a-C, 1961.
[24] A.M. Stoll, M.A. Chianta, Method and rating system for evaluation of thermal protection, Aero. Med. 40 (1969) 1232–1238.
[25] J. Smagorinsky, General circulation experiments with the primitive equations: I. The basic experiment, Mon. Weather Rev. 91 (1963) 99–164.
[26] S.K. Park, K.W. Miller, Random number generators: good ones are hard to find, Commun. ACM 31 (1988) 1192–1201.
[27] S. Zama, Damage of oil storage tanks due to the 2003 Tokachi-oki earthquake and revision of design spectra for liquid sloshing, Butsuri-Tansa 59 (2006) 353–362 (in Japanese).
[28] Fire Departments of Kesennuma and Motoyoshi, Report on Firefighting Activities Following the 2011 Great East Japan Earthquake, 2012. http://www.km-fire.jp/images_higashi/higashikatudou.pdf. (Accessed 11 September 2019).
[29] Cabinet Office, Government of Japan, Tsunami Source Model Parameters for the Tonankai-Nankai Earthquake, 2016. https://www.geospatial.jp/ckan/dataset/1890. (Accessed 11 September 2019).
[30] The Headquarters for Earthquake Research Promotion, Long-term Evaluation of Earthquakes in the Nankai Trough, second ed., 2013. http://www.jishin.go.jp/main/chousa/13may_nankai/index.htm. (Accessed 11 September 2019).
[31] S. Zama, Earthquake and oil storage tank (part 2): damage of hazardous materials facilities and seismic ground motions in the 1964 Niigata earthquake, Saf. Tomorrow 174 (2017) 38–45 (in Japanese).
[32] W.P. Kyaw, L. Junlin, Y. Takagi, H. Suzuki, N. Kato, Experimental and numerical analysis of tsunami triggered oil spill from storage tanks, in: Proceedings of the 27th International Ocean and Polar Engineering Conference, International Society of Offshore and Polar Engineers, 2017, pp. 673–680.